A Novel Three-phase Isolated *LLC* and Non-isolated *LCL-T* Resonant Converter for Fuel Cell Applications

Erdem Asa, Vivek Sujan, Omer C. Onar
Oak Ridge National Laboratory, National Transportation Research Center, Tennessee, USA
E-mail: asae@ornl.gov

Abstract — **In this paper, a novel three-phase isolated *LLC* and non-isolated *LCL-T* resonant converter topologies are introduced for fuel cell applications. In order to improve the fuel cell DC/DC converter efficiency, the current amplitude should be reduced in the power stage components. Cascaded connections of fuel cell blocks through a controllable system enable using higher voltage amplitude and bring the current amplitude lower at the target power. In this way, power losses in the passive components can be reduced, and maximum energy transfer can be established, improving the DC/DC converter efficiency from the fuel cell to the load. The introduced new converter also achieves soft switching (ZVS), minimizing the switching losses in all input and output load conditions. The presented three-phase isolated *LLC* and non-isolated *LCL-T* resonant converter systems, fed by three fuel cell modules with an output range of 190-380 V, deliver 580-730 V at 450 kW maximum output power. The results reveal that the proposed systems have the advantage of reducing the size, volume, and weight and increasing the overall DC/DC converter system efficiency compared to the single-phase systems.**

Keywords — three-phase, isolated, LLC, non-isolated, LCL-T resonant, converter, fuel-cell

I. INTRODUCTION

The growing demand for renewable energy sources has propelled the development of advanced power conversion systems, particularly in applications involving fuel cells [1]-[2]. Fuel cells are increasingly recognized for their potential in distributed generation and sustainable transportation due to their high efficiency, high energy density, low emissions, and ability to produce scalable power [3]-[4]. Integration of fuel cell stacks for high-power applications is a challenge. Authors informed in [5] that a series connection of fuel cell stacks without a controller decreases the fuel cell lifetime.

To address these challenges, this paper presents the design and analysis of a novel power converter tailored for fuel cell applications. The proposed converter connects fuel cell stacks in series with a controller and is optimized for three-phase systems, leveraging a resonant compensation network with isolated and non-isolated options to enhance performance. By operating above the resonant frequency, the system achieves zero-voltage switching (ZVS) for all power switches, significantly reducing switching losses and thermal stress. Furthermore, the system's operation minimizes reactive currents in the resonant tank, improving efficiency.

The comprehensive evaluation of the proposed system includes design calculations and validation through theoretical and PLECS simulations for an input range of 190-380 V and an output range of 580-730 V at 450 kW maximum output power. A power loss breakdown comparison is also provided to demonstrate the converter's practical feasibility and performance with parallel connection under maximum output power conditions. These contributions underscore the potential of the proposed converter to address critical inefficiencies in fuel cell integration, advancing the development of sustainable and efficient energy systems.

II. THE PROPOSED NOVEL THREE-PHASE ISOLATED *LLC* AND NON-ISOLATED *LCL-T* RESONANT CONVERTER

The proposed three-phase isolated *LLC* and non-isolated *LCL-T* resonant converter topology for fuel cell applications is shown in Fig. 1. As illustrated in the figure, the topology comprises H-bridge high-frequency inverter modules and cascaded fuel cell stacks connected via intercell transformers. In the designed three-phase system, one phase of each H-bridge power module is directly connected, while the remaining two phases are linked through intercell transformers, which establish a delta connection and facilitate the series connection of individual fuel cell stacks.

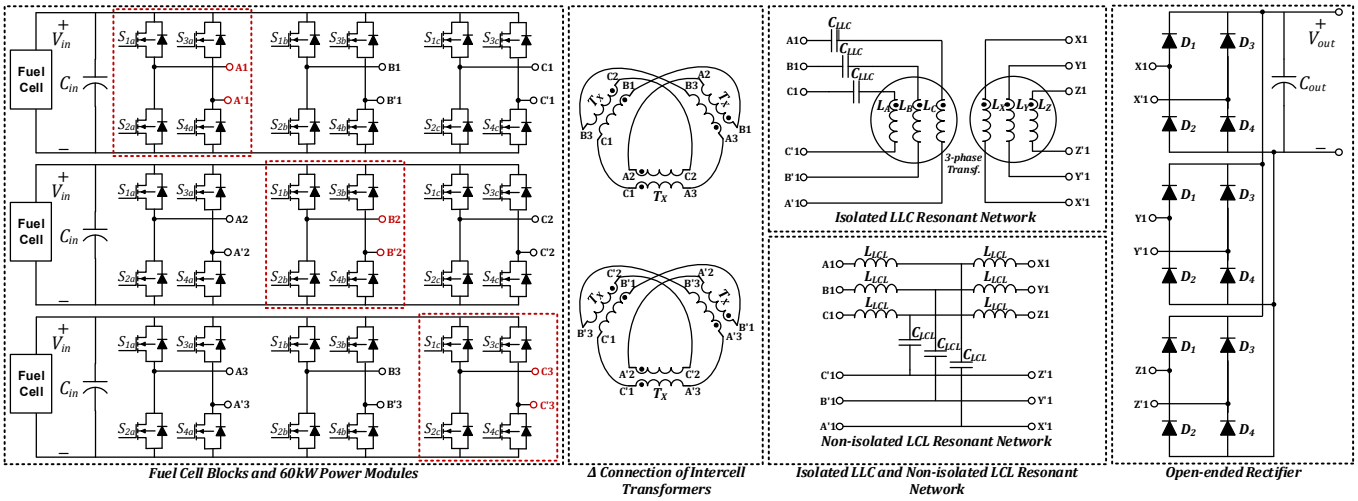

Fig. 1. The proposed novel three-phase isolated *LLC* and non-isolated *LCL-T* resonant converter structure.

The three-phase isolated *LLC* resonant network consists of series capacitors C_{LLC} and a three-phase transformer. Conversely, the three-phase non-isolated *LCL-T* resonant network features a T-connection with series inductors L_{LCL} and parallel capacitors C_{LCL}. Each phase output is rectified using an H-bridge rectifier and connected in parallel to the output load. Assuming identical converter parameters for each phase, the system's behavior can be analyzed using the single-phase equivalent circuit for isolated *LLC* resonant compensation [6]-[7] and non-isolated *LCL-T* resonant network shown in Fig. 2.

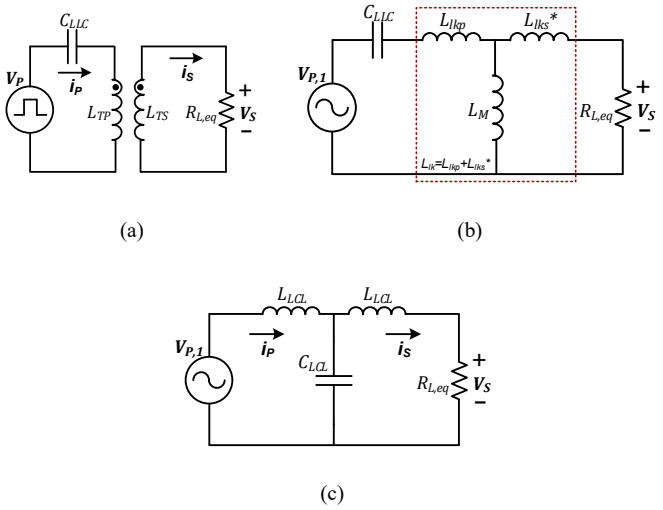

Fig. 2. Single phase; a) equivalent circuit and b) simplified circuit diagram for isoltaed *LLC* resonant network, c) simplified circuit diagram for non-isolated *LCL-T* resonant network.

The characteristic of the system is examined by describing the single-phase circuit models in Fig. 2. The primary side resonant tank voltage V_P is expressed as,

$$V_P = \frac{6\sqrt{2}}{\pi} V_{in} \tag{1}$$

The resonant tank currents I_P and I_S are written as,

$$I_P = \frac{\pi}{6\sqrt{2}} \frac{P_O}{\eta V_{in}} \tag{2}$$

$$I_S = \frac{\pi}{2\sqrt{2}} \frac{P_O}{V_{out}} \tag{3}$$

The load equivalent resistance $R_{L,eq}$ can be expressed by,

$$R_{L,eq} = \frac{8}{\pi^2} \frac{V_{out}^2}{P_O} \tag{4}$$

The corner cutoff resonant frequency $\omega_{O,LLC}$ and $\omega_{O,LCL}$ for *LLC* and *LCL-T* resonant networks is identified at full load considerations as, respectively,

$$\omega_{O,LLC} = \frac{1}{\sqrt{L_{lk} C_{LLC}}} \tag{5}$$

$$\omega_{O,LCL} = \frac{L_{LCL}}{\sqrt{2 L_{LCL} C_{LCL} (L_{LCL}^2 + C_{LCL}^2)}} \tag{6}$$

where L_{lk} is the transformer equivalent leakage inductance from the primary side $j\omega L_{lk} = \{j\omega L_{lkp} + j\omega L_{lks}^*\}$ for the *LLC* resonant network. The system critical resonant frequency $\omega_{C,LLC}$ for *LLC* and $\omega_{C,LCL}$ for *LCL-T* are quantified at no load condition and can be described as, respectively,

$$\omega_{C,LLC} = \frac{1}{\sqrt{L_M C_{LLC}}} \tag{7}$$

$$\omega_{C,LCL} = \frac{2}{\sqrt{L_{LCL} C_{LCL}}} \tag{8}$$

The proposed system's single-phase equivalent input and output impedances can be described for *LLC* and *LCL-T* resonant networks in matrix form as, respectively,

$$\begin{bmatrix} V_P \\ V_S \end{bmatrix} = \begin{bmatrix} \frac{1}{j\omega C_{LLC}} + j\omega(L_{lkp} + L_M) & -j\omega L_M \\ -j\omega L_M & j\omega(L_M + L_{lks}) + R_{L,eq} \end{bmatrix} \begin{bmatrix} I_P \\ I_S \end{bmatrix} \tag{9}$$

$$\begin{bmatrix} V_P \\ V_S \end{bmatrix} = \begin{bmatrix} j\omega L_{LCL} + \frac{1}{j\omega C_{LCL}} & -\frac{1}{j\omega C_{LCL}} \\ -\frac{1}{j\omega C_{LCL}} & \frac{1}{j\omega C_{LCL}} + j\omega L_{LCL} + R_{L,eq} \end{bmatrix} \begin{bmatrix} I_P \\ I_S \end{bmatrix} \tag{10}$$

The voltage gains transfer function of the *LLC* and *LCL-T* resonant network systems is found as, respectively,

$$M_V = \frac{V_S}{V_P} = \left| \frac{(j\omega L_M)//(j\omega L_{lkS}+R_{L,eq})}{\frac{1}{j\omega C_{LLC}}+j\omega L_{lkp}+[(j\omega L_M)//(j\omega L_{lkS}+R_{L,eq})]} \right| \quad (11)$$

$$M_V = \frac{V_S}{V_P} = \left| \frac{\left(\frac{1}{j\omega C_{LCL}}\right)//(j\omega L_{LCL}+R_{L,eq})}{j\omega L_{LCL}+\left[\left(\frac{1}{j\omega C_{LCL}}\right)//(j\omega L_{LCL}+R_{L,eq})\right]} \right| \quad (12)$$

III. System Design Optimization and Parameters

The system design optimization is proceeded by using the single stack fuel cell output conditions as given in Fig. 4. As seen from the figure, the fuel cell output voltage drops non-linearly; however, the stack output can be modeled in the linear region between maximum nominal output voltage and minimum output voltage regions as shown in Fig. 3. Also, the system output power behaves linearly in this area.

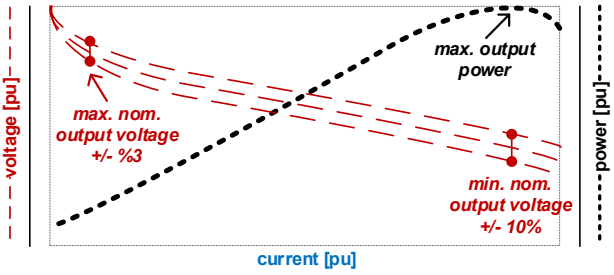

Fig. 3. Fuel Cell stack output voltage and power.

By using the fuel cell stack output voltage and power, the designed system fuel cell output conditions are summarized in Table I.

TABLE I – The System Design Conditions

Symbol	Parameter	Value
V_{min}	min. output voltage range	190-210 V (+/- %5)
V_{max}	max. output voltage range	270-380 V (+/- %15)
V_{min_nom}	min. nominal output voltage	190 V
V_{max_nom}	max. nominal output voltage	380 V
P_{max_nom}	max. nominal output power	150 kW

The designed DC/DC converter output connects to the traction inverter and battery. The output voltage range of the converter system is between 580-730 V, and the battery maintains the output voltage. For the isolated *LLC* resonant converter, the designed resonant tank parameters are calculated by using above design equations and the voltage gains transfer function below. The required leakage inductance L_{lk} of *LLC* transformer should allow the maximum resonant tank current amplitude at the resonant frequency f_r and is calculated as,

$$L_{lk} = \frac{4(V_{in}^2\eta+n^2V_{out}^2)}{\pi^3 f_r P_O} \quad (13)$$

where "n" is the transformer turn ratio between the primary and secondary sides for *LLC* resonant transformer. The voltage gain transfer function of the *LLC* resonant converter with the ratio between leakage L_{lk} and mutual inductance L_m of "A" ($A=L_m/L_{lk}$) and normalized frequency f_n ($=f_{sw}/f_r$) is demonstrated in Fig. 4.

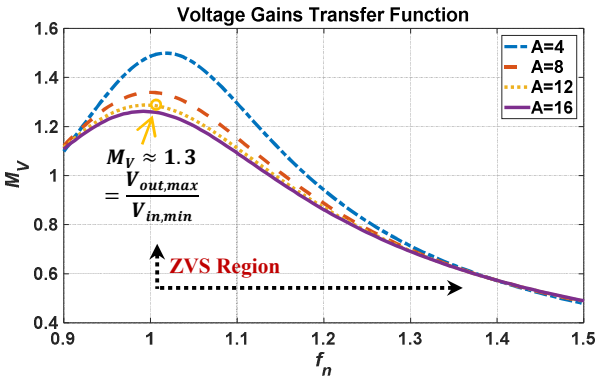

Fig. 4. The voltage gains transfer function of the *LLC* resonant converter.

As shown in the figure, the system's voltage gain transfer function can be initiated at the resonant frequency with the minimum input voltage (corresponding to a three-stack series connection of fuel cell blocks) and the maximum output voltage by controlling the system's operating frequency. As the parameter "A" increases from 4 to 16, the gain curve becomes more linear, and the system's frequency sensitivity decreases; however, this also results in a reduction in the gain amplitude. Therefore, a higher value of "A" is recommended to ensure sufficient gain while maintaining system controllability in a more linear region with reduced frequency sensitivity. In this design, setting "A" to 12 provides an adequate gain margin to achieve the desired input-to-output conversion within the controllable frequency range. The design transformer coupling factor can be found as,

$$k = \frac{L_m}{L_{lk}+L_m} \quad (14)$$

The transformer's primary and secondary side self-inductances L_{TP} and L_{TS} values can be obtained as,

$$L_{TP} = \frac{L_m}{k}\frac{I_S}{I_P} \quad (15)$$

$$L_{TS} = \frac{L_m}{k}\frac{I_P}{I_S} \quad (16)$$

The transformer's turns ratio can be expressed as,

$$n = \sqrt{\frac{L_{TP}}{L_{TS}}} \quad (17)$$

For the non-isolated *LCL-T* resonant converter, the required series inductance L_{LCL} value is stated as,

$$L_{LCL} = \frac{4V_{in}^2\eta}{\pi^3 f_r P_O} \quad (18)$$

The quantified resonant power stage component values are presented for isolated *LLC* and non-isolated *LCL-T* in Table II.

TABLE II – The Resonant Network Values

Symbol	Parameter	Value
L_{TX}	Intercell transformer self-inductance	10 µH
	Isolated *LLC* Resonant Converter	
C_{LLC}	Resonant series capacitor	625 nF
L_{lk}	Transformer leakage inductance	11 µH
k	Coupling co-efficient	0.923
L_m	Transformer mutual inductance	132 µH
L_{TP}	Transformer primary self-inductance	108 µH
L_{TS}	Transformer secondary self-inductance	189 µH
n	Transformer turns ratio	0.76
	Non-isolated *LCL-T* Resonant Converter	
C_{LLC}	Resonant parallel capacitor	1.87 µF
L_{LCL}	Resonant series inductor	5.42 µH

The calculated intercell transformer self-inductance values are found considering the input equivalent voltage and power for each output of the H-bridge inverter that can compensate the circulating current between H-bridges.

IV. The Proposed System Theoretical and PLECS Simulation Results and Comparison Analysis

The proposed systems theoretical and PLECS simulation results are presented for isolated *LLC* and non-isolated *LCL-T* resonant converters. Fig. 5 demonstrates the results for the isolated *LLC* resonant converter.

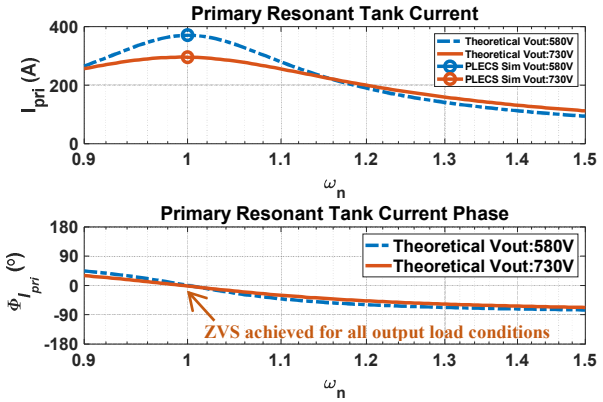

(a)

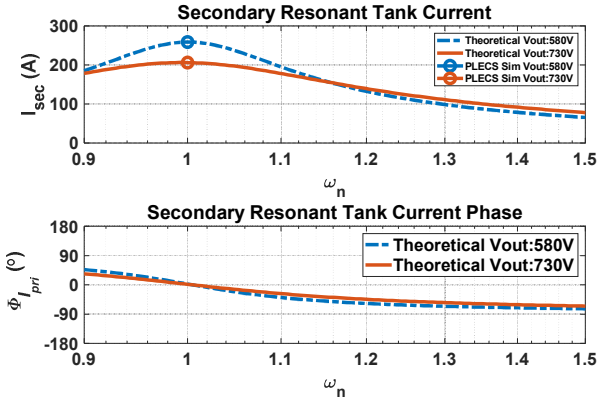

(b)

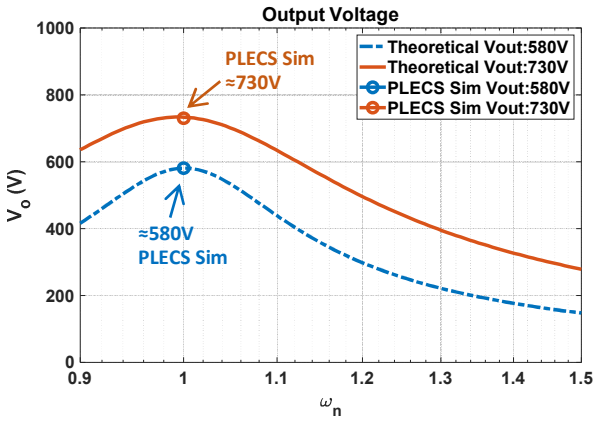

(c)

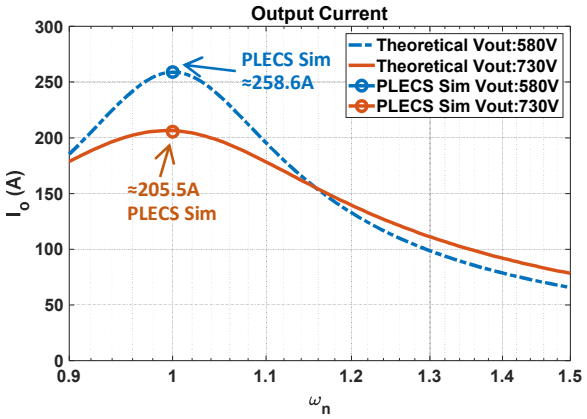

(d)

Fig. 5. Isolated *LLC* resonant converter theoretical and PLECS simulation results; (a) primary side resonant tank current I_{pri} and phase ϕI_{pri}, (b) secondary side resonant tank current I_{sec} and phase ϕI_{sec} (c) output voltage V_O, (d) output current I_O.

The plotted graphs illustrate the primary and secondary side resonant current and phase, output voltage, and current with circular markers representing PLECS simulation results. The theoretical and PLECS simulation results for the non-isolated *LCL-T* resonant converter are shown in Fig. 6.

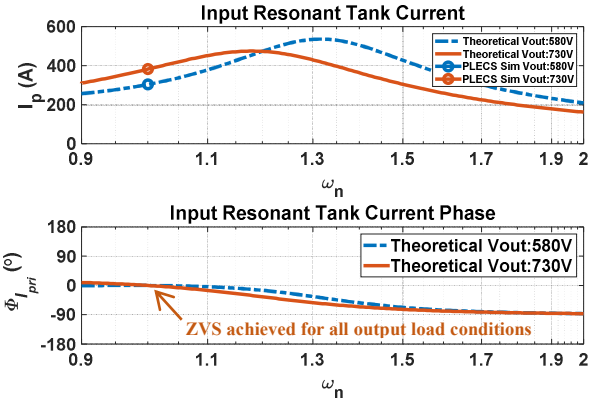

(a)

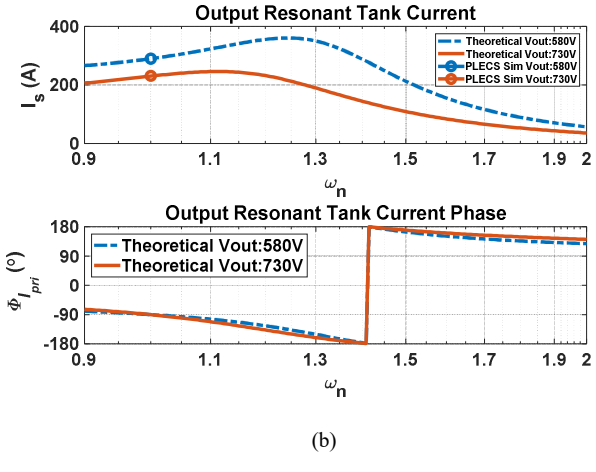

(b)

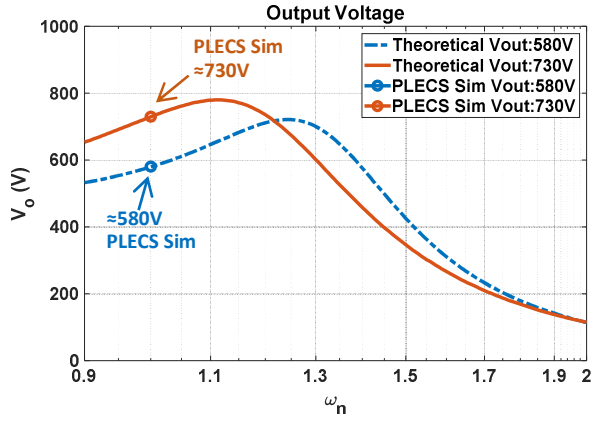

(c)

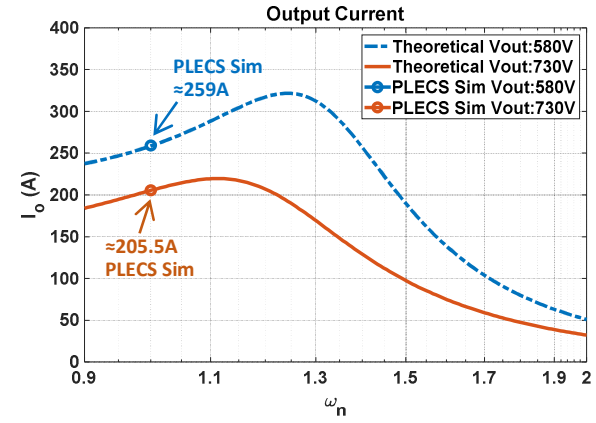

(d)

Fig. 6. Non-isolated *LCL-T* resonant converter theoretical and PLECS simulation results; (a) input resonant tank current I_p and phase ϕI_p, (b) output resonant tank current I_s and phase ϕI_s, (c) output voltage V_O, (d) output current I_O.

As seen from the results, the perfect alignment between theoretical and simulation results confirms the accuracy of the proposed analysis method for isolated *LLC* and non-isolated *LCL-T* resonant networks. Additionally, zero-voltage switching (ZVS) is achieved in the primary-side inverter, as the input resonant tank current remains below *"0"* degrees for all angular frequencies above the resonant frequency, reducing switching losses and improving efficiency. This validation confirms the effectiveness of the proposed system in accurately predicting circuit behavior and ensuring optimal performance under varying operating conditions.

To evaluate the system efficiency, the overall power component selections are detailed along with the system subcomponents, considering 50 kW power modules for each H-bridge inverter. Thermal analysis is performed to guide the selection and design of all subcomponents under ambient temperature conditions of 45°C. The selected and custom-designed components are summarized in Table III.

TABLE III – System Selected Sub-components

	Component	Part Number
H-Bridge Inverter	SiC MOSFET module	Wolfspeed CAB400M12XM3
	Gate driver	Wolfspeed CGD12HBXMP
	Liquid-cooled cold plate	Microcool CP 4012D MDT XP
Rectifier	SiC schottky diode	GeneSiC GC50MPS12-247
	Liquid-cooled cold plate	ATS-TCP-1004
Resonant Tank for LLC	Series resonant capacitor	CELEM CSP (custom)
	Intercell transformer	Ferroxcube E100/60/28-3C95 ferrite core
	Transformer	Payton planar transformer (custom made)
Resonant Tank for LCL-T	Series inductor	Ferroxcube E100/60/28-3C95 ferrite core
	Parallel capacitor	CELEM CSP (custom)

Each system's power loss analysis is conducted based on the selected and designed subcomponents listed in Table III, considering thermal analysis at the maximum output power of 450 kW (three fuel cell stacks, each rated at 150 kW) and a nominal output voltage of 660 V. Unlike the proposed converters, which follow a *series-parallel* configuration with intercell transformers, two alternative system designs with a single-phase *parallel* connection (without intercell transformers) are considered for comparison — one using an isolated single-phase parallel *LC* resonant converter and the other using a non-isolated single-phase parallel *LC* resonant converter. The efficiency comparison between the proposed *series-parallel* configurations with intercell transformer and these *parallel* configurations is presented in Table IV.

TABLE IV – Efficiency Comparison Analysis

System	Resonant Network	Configuration	Efficiency (%)
Isolated	Three-phase *LLC*	*series-parallel (proposed)*	98.01
	Sigle-phase *LC*	*parallel*	96.62
Non-isolated	Three-phase *LCL*	*series-parallel (proposed)*	98.24
	Single-phase *LC*	*parallel*	97.22

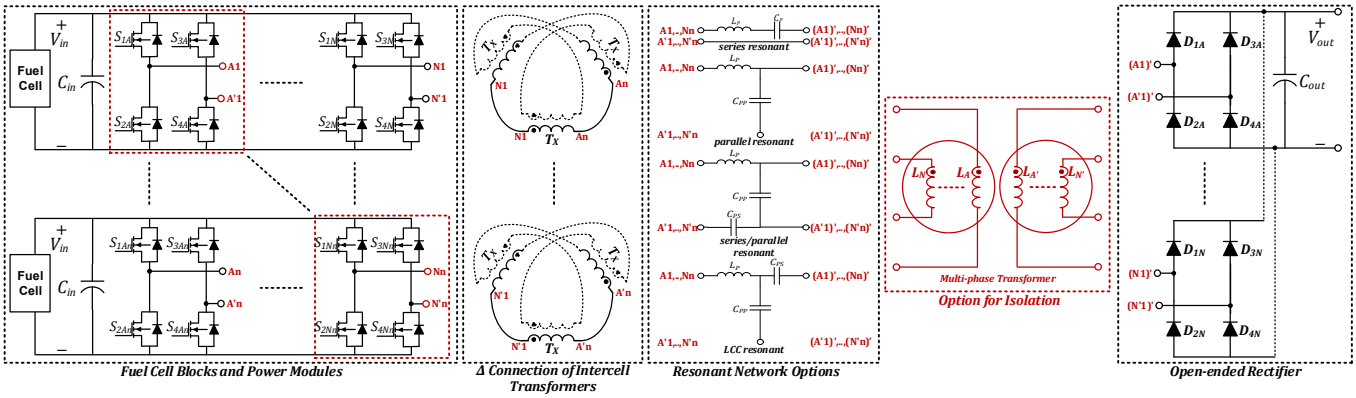

Fig. 7. The proposed novel multi-phase isolated and non-isolated resonant converter structure with different resonant networks.

As seen from the results, the proposed converter topologies for both isolated and non-isolated configurations offer a clear advantage in terms of component count and power loss compared to the parallel connection systems. At the maximum output power of 450 kW, the expected overall efficiency of the isolated three-phase *LLC* resonant converter is approximately 98.01%, while that of the non-isolated three-phase *LCL-T* resonant converter is 98.24%. These results indicate that the efficiency of the isolated system can be improved by approximately 1.39%, and the efficiency of the non-isolated system can be improved by approximately 1.02%.

V. Conclusions

In this paper, a novel isolated three-phase *LLC* resonant converter and non-isolated three-phase *LCL-T* resonant converter topologies are introduced specifically for fuel cell applications, addressing critical challenges in efficiency and power management for high-power systems. By employing a resonant compensation network and cascaded connections of fuel cell stacks through a controllable system, the proposed converter successfully reduces current amplitudes in power stage components, thereby minimizing power losses and enhancing energy transfer efficiency. The system demonstrates significant advantages, including achieving zero-voltage switching (ZVS) across all input and output load conditions, effectively reducing switching losses. With its ability to operate over a wide output voltage range of 580-730 V and deliver up to 450 kW of maximum output power, the three-phase design proved superior to single-phase systems, offering reductions in size, volume, and weight while enhancing overall efficiency. Simulation and analysis results validated the system's performance, highlighting its potential to maximize the energy efficiency of DC/DC conversion from fuel cells to loads in demanding applications.

The proposed system with different resonant compensation networks and multi-phase transformer winding configuration (as an option for isolation) is presented considering the multi-phase connection of fuel-cell stacks in Fig. 7. In this way, multi-phase fuel-cell stack systems can be connected through the proposed system with the different resonant network options rather than three-phase isolated *LLC* and non-isolated *LCL-T* resonant compensation.

Acknowledgements

This research used the resources available at the Power Electronics and Electric Machinery (PEEM) laboratory at the National Transportation Research Center (NTRC), a U.S. Department of Energy (DOE) Office of Energy Efficiency and Renewable Energy (EERE) user facility operated by Oak Ridge National Laboratory (ORNL). Authors would like to thank Dr. William Gibbons (Hydrogen and Fuel Cell Technologies Office, U.S. Department of Energy) and Lee Slezak (Vehicle Technologies Office, U.S. Department of Energy) for funding this work and for their continuous support and guidance.

References

[1] S. H. Son, C. H. Kwon, T. H. Kim, C. H. Yu, S. R. Jang, E. S. Kim, H. S. Kim, "Optimal Design of LCC Resonant Converter With Phase Shift Control for Wide Input/Output Voltage Ranges in Fuel Cell System," *IEEE Transactions on Industrial Electronics*, vol. 71, no. 4, pp. 3537-3547, Apr. 2024.

[2] A. U. Rehman, S. W. Ryu, H. Park, J. W. Jung, "A Critical Review of Recent Industrial Developments, Trends, and Future Perspectives of Power Electronic Systems: Fuel Cell Electric Vehicles," *IEEE Transactions on Industrial Informatics*, vol. 20, no. 4, pp. 6060-6074, Apr. 2024.

[3] Z. Wang, Z. Zheng, C. Li, "A High-Step-Up Low-Ripple and High-Efficiency DC-DC Converter for Fuel-Cell Vehicles," *IEEE Transactions on Power Electronics*, vol. 37, no. 3, pp. 3555-3569, Mar. 2022.

[4] H. N. Tran, T. T. LE, H. Jeong, S. Kim, S. Choi, "A 300 kHz, 63 kW/L ZVT DC–DC Converter for 800-V Fuel Cell Electric Vehicles," *IEEE Transactions on Power Electronics*, vol. 37, no. 3, pp. 2993-3006, Mar. 2022.

[5] N. Marx, J. Cardozo, L. Boulon, F. Gustin, D. Hissel, K. Agbossou, "Comparison of the Series and Parallel Architectures for Hybrid Multi-Stack Fuel Cell - Battery Systems," *IEEE Vehicle Power and Propulsion Conference (VPPC)*, Montreal, QC, Canada, 2015.

[6] E. Asa, K. Colak, M. Bojarski, D. Czarkowski, "Three phase LLC resonant converter with D-DLL control technique for EV battery chargers," *IEEE International Electric Vehicle Conference (IEVC)*, Florence, Italy, 2014, pp. 1-7.

[7] K. Colak, E. Asa, D. Czarkowski, "A comparison analysis of CLL and LLC resonant converter for multi-phase applications," *IEEE Transportation Electrification Conference and Expo (ITEC)*, Dearborn, MI, USA, 2015, pp. 1-6.